

# LATENT EQUIVARIANT OPERATORS FOR ROBUST OBJECT RECOGNITION: PROMISE AND CHALLENGES

**Minh Dinh**

Department of Computer Science  
Dartmouth College  
Hanover, NH 03755, USA  
Minh.T.Dinh.GR@dartmouth.edu

**Stéphane Deny**

Departments of Computer Science &  
Neuroscience and Biomedical Engineering  
Aalto University, Espoo, Finland  
stephane.deny.pro@gmail.com

## ABSTRACT

Despite the successes of deep learning in computer vision, difficulties persist in recognizing objects that have undergone group-symmetric transformations rarely seen during training—for example objects seen in unusual poses, scales, positions, or combinations thereof. Equivariant neural networks are a solution to the problem of generalizing across symmetric transformations, but require knowledge of transformations *a priori*. An alternative family of architectures proposes to *learn equivariant operators* in a latent space from *examples* of symmetric transformations. Here, using simple datasets of rotated and translated noisy MNIST, we illustrate how such architectures can successfully be harnessed for out-of-distribution classification, thus overcoming the limitations of both traditional and equivariant networks. While conceptually enticing, we discuss challenges ahead on the path of scaling these architectures to more complex datasets.

## 1 INTRODUCTION

Deep networks have progressed to match or even outperform humans on many image recognition benchmarks (He et al., 2015; Vasudevan et al., 2022; Deghani et al., 2023). However, deep networks mostly excel on testing sets which are *identically distributed* (iid) to the training set. This high performance on iid benchmarks is not necessarily indicative of their performance in scenarios that have rarely been visited during training, in the so-called *out-of-distribution* domain. For example, state-of-the-art deep networks have shown to be brittle on tasks of recognizing objects in unusual poses, scales, or positions (Alcorn et al., 2019; Madan et al., 2021; Ibrahim et al., 2022; Madan et al., 2022; Abbas & Deny, 2023; Ollikka et al., 2025). Such scenarios can often be described in the language of *group theory*: changes of pose, scale, and position are indeed the result of *group transformations* acting on visual objects.

Several approaches have been proposed to increase robustness of deep networks to group transformations that are absent or only partially present in the training dataset. First, **equivariant neural networks** offer guarantees of robustness to target group transformations (Cohen et al., 2019; Bekkers, 2019). However, transformations need to be pre-specified mathematically in order to construct the relevant architecture for them. Second, **data augmentations schemes**, used in combination with either supervised or self-supervised learning objectives (e.g., Benton et al., 2020; Zbontar et al., 2021; Brehmer et al., 2024), can ensure some level of invariance to pre-specified transformations. However, for optimal results, transformations need to be sampled uniformly across the entire range of parameters seen at test time (Gerken & Kessel, 2024; Perin & Deny, 2025). This is not always possible, in particular when one is only given *examples* of transformations *in a limited range*. In a third line of work, methods have been proposed that learn group transformations from examples, hereafter referred to as **latent equivariant operator** methods (Culpepper & Olshausen, 2009; Sohl-Dickstein et al., 2017; Connor & Rozell, 2020; Dupont et al., 2020; Bouchacourt et al., 2021; Keller & Welling, 2021; LeCun, 2022; Connor et al., 2024). These methods learn an encoder jointly with a latent space operator, such that after training the latent space operator produces trans-

formations that are approximately equivariant to the transformations present in the dataset. These methods offer a promising alternative for out-of-distribution object recognition.<sup>1</sup>

**Here, we illustrate how equivariant latent operator methods can successfully be applied to out-of-distribution classification problems.** For simplicity, we strip down the complexity of the datasets and models to their minimal components necessary to establish the superiority of these methods over others. On rotated and translated noisy MNIST, we train a neural encoder jointly with a latent operator to learn equivariance over a limited range of transformations. At the same time, we train a classifier, taking as input the latent space, on the same range of transformations. At inference time, we test our model over a range of transformations that were not seen during training, assessing its extrapolation and composition abilities. We use a K-nearest-neighbour strategy to select the operator action most likely to revert the object back to its canonical pose. We establish the superiority of our method over comparable architectures on classifying inputs outside the training range. We conclude with a discussion on the challenges that are expected when scaling these methods to more complex datasets.

## 2 METHODS

**Dataset** We present experiments on a task of MNIST digit classification (LeCun et al., 2010). We extract the digit by thresholding pixel intensities above 128, recolor the digit in blue, and place it onto a random black-and-white checkerboard background, acting as noise to be ignored by the classifier. The digit is transformed by either a rotation or X-Y translations. Rotations are discretized in steps of  $36^\circ$ , yielding 10 distinct elements. Translations use a stride of 2 pixels along each axis on the  $28 \times 28$  grid (with periodic boundary condition), resulting in a translation group of order 14 per axis. Variants of the same digit share the same noise background. To avoid confusion with class ‘6’ when rotating, we exclude class ‘9’ from the dataset.

**Architecture** We use a simple feed-forward architecture. The encoder consists of a single linear layer that maps the flattened input into a latent representation to be transformed with the shift operator. When there are a combination of transformations, we use stacked encoders and operators for each transformation. We set the latent dimensionality to 70 to accommodate the orders of the transformation groups considered. The **pre-defined** latent operator follows the discrete construction of Bouchacourt et al. (2021): each block has a size equal to the order of the corresponding transformation group and is repeated along the diagonal to match the latent dimensionality. To evaluate whether equivariance can be learned from scratch, we also consider a **learnable** operator variant initialized as the Q factor of a QR decomposition (to ensure orthogonality) of a randomly sampled matrix. A classifier, stacked after the encoder, is a two-layer MLP with a sigmoid nonlinearity in the hidden layer, producing class logits from the transformed latent features. Further details are provided in Appendix A.

**Training** Given a training sample  $(x, y)$ , we generate two views by applying discrete transformations parameterized by  $k_1$  and  $k_2$ :  $x_1 = T^{k_1}(x)$ ,  $x_2 = T^{k_2}(x)$ , where  $T$  denotes a group transformation family and  $k_1, k_2$  are sampled transformation parameters. As illustrated in Figure 1, each transformed view is first mapped to a canonical representation using the corresponding inverse shift operator. Specifically, the two views’ canonicalized embeddings are obtained as

$$Z_1 = \varphi^{-k_1} f_E(x_1), \quad Z_2 = \varphi^{-k_2} f_E(x_2).$$

We encourage consistency between the learned representations by minimizing the distance between these canonical embeddings:

$$\mathcal{L}_{\text{reg}} = \|Z_1 - Z_2\|_2^2. \tag{1}$$

The canonicalized representation of the first view is fed to the classifier head:

$$\mathcal{L}_{\text{CE}} = \text{CrossEntropy}(f_D(Z_1), y).$$

---

<sup>1</sup>Latent equivariant operator methods should be distinguished from disentanglement methods; the latter can be seen as special cases of the former, where the latent operator is confined to a subspace (Higgins et al., 2018)—but see topological defects induced by subspace disentanglement in Bouchacourt et al. (2021).

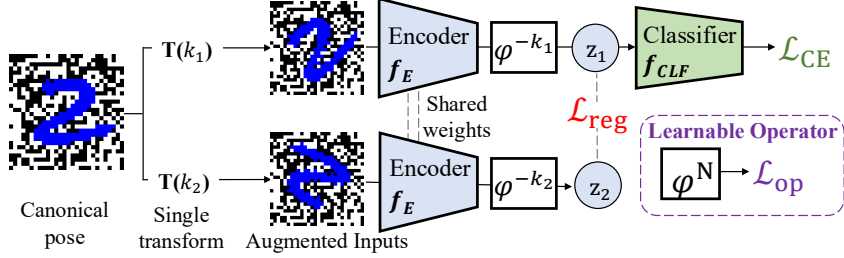


Figure 1: **Pipeline for handling single transformation.** Two transformed views of the same input are encoded by a shared encoder  $f_E$  and mapped to a canonical representation using inverse shift operators  $\varphi^{-k_1}$  and  $\varphi^{-k_2}$ , yielding embeddings  $Z_1$  and  $Z_2$ . The embedding  $Z_1$  is used for classification via a MLP  $f_{CLF}$  optimized with the cross-entropy loss  $\mathcal{L}_{CE}$ , while a representation consistency loss  $\mathcal{L}_{reg}$  encourages alignment between  $Z_1$  and  $Z_2$  that both correspond to the canonical pose. When the operator is learned, we add an extra term  $\mathcal{L}_{op}$  to the loss.

The final training objective is

$$\mathcal{L} = \mathcal{L}_{CE} + \lambda \mathcal{L}_{reg}, \quad (2)$$

where  $\lambda$  controls the strength of the regularization. When using a learnable operator, we aim to preserve the periodic properties of the operator by adding to the objective in Equation 2 another term that encourages the periodicity of the operator group:

$$\mathcal{L}_{op} = \|\varphi^N - I\|_2, \quad (3)$$

where  $N$  is the order (number of unique elements) of the group represented by the operator. Throughout all experiments, the order of our learnable operator was set to 70, equal to the latent dimensionality, which is substantially larger and did not need to be tailored to the true period of the underlying transformation (e.g., 10 for rotations or 7 for translations).

**Inference** In the absence of explicit transformation labels at inference time, we infer the pose of an input via a  $K$ -nearest neighbor (k-NN) search over a reference set of canonical embeddings. We first construct a class-agnostic reference database by collecting  $N$  validation samples  $x_j$  with known transformation indices  $\ell_j$  and mapping them back to a canonical pose using the inverse operator:

$$\mathcal{R} = \{r_j = \varphi^{-\ell_j} f(x_j)\}_{j=1}^N.$$

Given a test input  $x$ , we evaluate its embedding under each candidate transformation operator  $\{\varphi_\ell\}$ :

$$z_\ell = f(\varphi_\ell(x)), \quad \ell \in \mathcal{G},$$

where  $\mathcal{G}$  denotes the set of discrete transformation indices. We compute Euclidean distances between each transformed embedding  $z_\ell$  and all reference embeddings  $r_j \in \mathcal{R}$ . The predicted transformation index is obtained by majority voting over the indices associated with the  $K$  nearest reference matches:

$$\hat{\ell} = \text{mode}(\text{Top}K(\{\|z_\ell - r_j\|_2\}_{\ell,j})), \quad (4)$$

where  $\text{Top}K(\cdot)$  returns the transformation indices corresponding to the  $K$  smallest distances among all reference comparisons. The embedding  $z_{\hat{\ell}}$  is then selected and passed to the classifier.

### 3 RESULTS

All implementation details are provided in Appendix B.

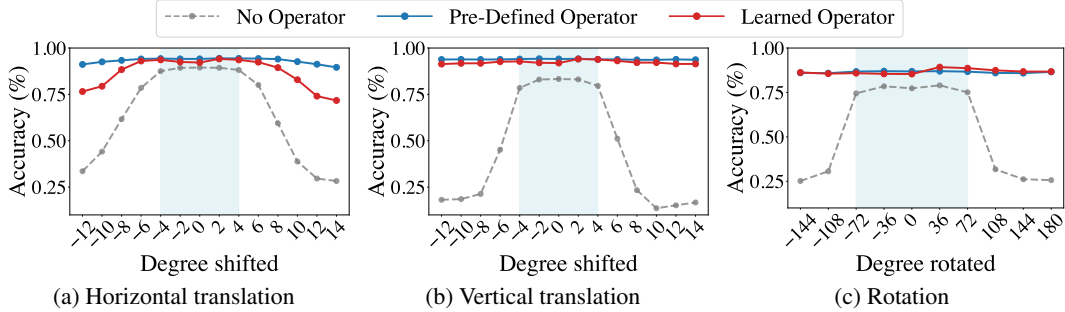


Figure 2: **Classification accuracy as a function of transformations on MNIST.** The shaded region denotes the range of translations observed during training.

**Performance on unseen degrees of a single transformation** We designate a subset of transformations as in-domain during training. For rotations, we use angles of  $\{-72^\circ, -36^\circ, 0^\circ, 36^\circ, 72^\circ\}$ . For translations, we use shifts by  $\{-4, -2, 0, 2, 4\}$  pixels. Figure 2 illustrates classification accuracy as a function of horizontal translation, vertical translation, and rotation. For the baseline model—a model with the same encoder-classifier architecture but in which no operator was applied during training or inference—accuracy peaks within the training range and decreases sharply as inputs move further into unseen transformations, forming a pronounced bell-shaped curve. In contrast, models equipped with latent operators exhibit nearly flat accuracy profiles across the entire transformation range, indicating stable extrapolation. The learned-operator variants show similar trends, with slightly increased variance in accuracy across degrees of transformation, suggesting that equivariant structure can be recovered even when the operator is learned rather than fixed. We report the exact numerical results in Appendix C.1, and an ablation on the k-NN method in Appendix C.2.

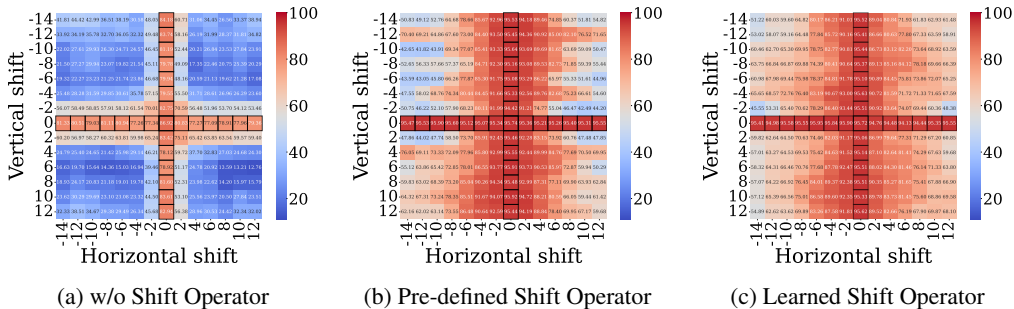


Figure 3: **Test accuracy heatmaps under joint horizontal (rows) and vertical (columns) translations.** The bordered cross indicates transformations observed during training.

**Performance on unseen combination of transformations** Figure 3 shows classification accuracy under joint horizontal and vertical translations, using the stacked operator version of our model. When no shift operator is used (Figure 3a), accuracy deteriorates rapidly outside the training region, indicating poor generalization to unseen translation combinations. In contrast, both the pre-defined (Figure 3b) and learned (Figure 3c) shift operators generalize well beyond the training cross, maintaining high accuracy across most unseen combinations. Notably, the learned shift operator attains comparable, and in some corner regions slightly higher accuracy than the pre-defined operator, suggesting that data-driven operator learning can recover effective equivariant structure without explicit specification.

#### 4 DISCUSSION

Here we demonstrated, in a minimal setup, how latent equivariant operators can be leveraged to classify out-of-distribution samples—by means of extrapolation and combination of symmetric transfor-

mations. Unlike in equivariant neural networks, the symmetries did not need to be mathematically pre-specified. Unlike in data augmentation schemes, the method did not require coverage of the full range of transformation parameters during training. Intuitively, this is because the recursive application of operators in latent space allows the extrapolation of transformations beyond the training range, and in unseen combinations. **Latent equivariant operator methods thus offer a promising avenue for robust, human-like<sup>2</sup> object recognition, and warrant further investigation.**

To date, latent equivariant operator methods have not been shown to scale to large and complex datasets in the out-of-distribution domain. **We identify a number of theoretical and implementation challenges ahead.** First, we do not know theoretically the certainty with which we can expect operators to remain equivariant beyond the training range of transformation parameters. Empirically, we find classification performance to degrade somewhat outside the training range. Moreover, we do not know at what layer of an architecture such operators should be situated. For the affine transformations explored in this minimal study, a single linear layer suffices to recast the representation in a way suitable to the operator (whether learned or fixed), as described in previous theory (Bouchacourt et al., 2021). For more complex transformations, for example transformations happening in a latent space not directly accessible from pixel space (e.g., in-depth 3D rotation), it is unclear how many layers would be required. Empirically, latent equivariant operators have been shown to successfully emulate in-depth 3D rotations (Dupont et al., 2020). Finally, the choice of the functional form of latent operators is another open question, involving fundamental notions in *representation theory* and *topology*. The resolution of these theoretical questions should provide guidance for the successful implementation of latent equivariant operator approaches at scale.

## ACKNOWLEDGMENTS

We thank members of the BRAIN lab at Aalto University, Ivan Vujaklija, Mansour Taleshi, and T. Andy Keller for useful discussions. This work was supported in part by the Academy of Finland under Grant 3357590 for S.D, and by the Helsinki Institute for Information Technology (HIIT) under Contract No. 9125064HIIT for M.D.T.

## REFERENCES

- Amro Abbas and Stéphane Deny. Progress and limitations of deep networks to recognize objects in unusual poses. *AAAI Conference on Artificial Intelligence*, 2023.
- Michael A Alcorn, Qi Li, Zhitao Gong, Chengfei Wang, Long Mai, Wei-Shinn Ku, and Anh Nguyen. Strike (with) a pose: Neural networks are easily fooled by strange poses of familiar objects. In *Conference on Computer Vision and Pattern Recognition (CVPR)*, 2019.
- Erik J Bekkers. B-spline cnns on lie groups. *arXiv preprint arXiv:1909.12057*, 2019.
- Gregory Benton, Marc Finzi, Pavel Izmailov, and Andrew G Wilson. Learning invariances in neural networks from training data. *Advances in Neural Information Processing Systems (NeurIPS)*, 33: 17605–17616, 2020.
- Diane Bouchacourt, Mark Ibrahim, and Stéphane Deny. Addressing the topological defects of disentanglement via distributed operators. *arXiv preprint arXiv:2102.05623*, 2021.
- Johann Brehmer, Sönke Behrends, Pim de Haan, and Taco Cohen. Does equivariance matter at scale?, 2024.
- Taco S Cohen, Mario Geiger, and Maurice Weiler. A general theory of equivariant cnns on homogeneous spaces. In *Advances in Neural Information Processing Systems (NeurIPS)*, volume 32, 2019.
- Marissa Connor and Christopher Rozell. Representing closed transformation paths in encoded network latent space. *AAAI Conference on Artificial Intelligence*, 34(04):3666–3675, 2020.

---

<sup>2</sup>Note that latent operators can be conceived as performing internal changes of perspective akin to mental simulation in humans (e.g., Shepard & Metzler, 1971; Khazoum et al., 2025).

- Marissa Connor, Bruno Olshausen, and Christopher Rozell. Learning internal representations of 3D transformations from 2D projected inputs. *Neural Computation*, 36(11):2505–2539, 2024.
- Benjamin Culpepper and Bruno Olshausen. Learning transport operators for image manifolds. *Advances in Neural Information Processing Systems (NeurIPS)*, 22:423–431, 2009.
- Mostafa Dehghani, Josip Djolonga, Basil Mustafa, Piotr Padlewski, Jonathan Heek, Justin Gilmer, and et al. Scaling vision transformers to 22 billion parameters. *International Conference on Machine Learning (ICML)*, 2023.
- Emilien Dupont, Miguel Bautista Martin, Alex Colburn, Aditya Sankar, Josh Susskind, and Qi Shan. Equivariant neural rendering. In *International Conference on Machine Learning (ICML)*, volume 119, pp. 2761–2770, 2020.
- Jan E Gerken and Pan Kessel. Emergent equivariance in deep ensembles. In *International Conference on Machine Learning (ICML)*, volume 235, pp. 15438–15465, 2024.
- Kaiming He, Xiangyu Zhang, Shaoqing Ren, and Jian Sun. Delving deep into rectifiers: Surpassing human-level performance on imagenet classification. *International Conference on Computer Vision (ICCV)*, 2015.
- Irina Higgins, David Amos, David Pfau, Sebastien Racaniere, Loic Matthey, Danilo Rezende, and Alexander Lerchner. Towards a Definition of Disentangled Representations. *arXiv:1812.02230*, December 2018. arXiv: 1812.02230.
- Mark Ibrahim, Quentin Garrido, Ari Morcos, and Diane Bouchacourt. The robustness limits of sota vision models to natural variation. *arXiv preprint arXiv:2210.13604*, 2022.
- T. Anderson Keller and Max Welling. Topographic vaes learn equivariant capsules. In *Advances in Neural Information Processing Systems (NeurIPS)*, volume 34, pp. 28585–28597, 2021.
- Raymond Khazoum, Daniela Fernandes, Aleksandr Krylov, Qin Li, and Stephane Deny. A deep learning model of mental rotation informed by interactive vr experiments. *arXiv preprint arXiv:2512.13517*, 2025.
- Yann LeCun. A path towards autonomous machine intelligence. *Position paper, Version 0.9.2*, 2022.
- Yann LeCun, Corinna Cortes, and CJ Burges. Mnist handwritten digit database. *ATT Labs [Online]*, 2, 2010.
- Spandan Madan, Tomotake Sasaki, Tzu-Mao Li, Xavier Boix, and Hanspeter Pfister. Small in-distribution changes in 3d perspective and lighting fool both cnns and transformers. *arXiv preprint arXiv:2106.16198*, 2021.
- Spandan Madan, Timothy Henry, Jamell Dozier, Helen Ho, Nishchal Bhandari, Tomotake Sasaki, Frédo Durand, Hanspeter Pfister, and Xavier Boix. When and how convolutional neural networks generalize to out-of-distribution category–viewpoint combinations. *Nature Machine Intelligence*, 2022.
- Netta Ollikka, Amro Kamal Mohamed Abbas, Andrea Perin, Markku Kilpeläinen, and Stephane Deny. A comparison between humans and AI at recognizing objects in unusual poses. *Transactions on Machine Learning Research (TMLR)*, 2025. ISSN 2835-8856.
- Andrea Perin and Stéphane Deny. On the ability of deep networks to learn symmetries from data: A neural kernel theory. *Journal of Machine Learning Research (JMLR)*, 2025.
- Roger N Shepard and Jacqueline Metzler. Mental rotation of three-dimensional objects. *Science*, 171(3972):701–703, 1971.
- Jascha Sohl-Dickstein, Ching Ming Wang, and Bruno A. Olshausen. An Unsupervised Algorithm For Learning Lie Group Transformations. *arXiv:1001.1027*, June 2017. arXiv: 1001.1027.
- Vijay Vasudevan, Benjamin Caine, Raphael Gontijo Lopes, Sara Fridovich-Keil, and Rebecca Roelofs. When does dough become a bagel? analyzing the remaining mistakes on imagenet. *Advances in Neural Information Processing Systems (NeurIPS)*, 2022.

Jure Zbontar, Li Jing, Ishan Misra, Yann LeCun, and Stéphane Deny. Barlow twins: Self-supervised learning via redundancy reduction. In *International Conference on Machine Learning (ICML)*, pp. 12310–12320. PMLR, 2021.

## A METHODOLOGY DETAILS

### A.1 PRELIMINARY ON SHIFT OPERATOR

**Model components.** We decompose the model into an encoder  $f_E : \mathcal{X} \rightarrow \mathcal{Z}$ , which maps an input  $x \in \mathcal{X}$  to a latent representation, and a classifier  $f_{\text{CLF}} : \mathcal{Z} \rightarrow \mathcal{Y}$ , which predicts the output label from the representation. Unless otherwise stated, all encoders are linear in this study.

We consider a family of discrete affine transformations that form a cyclic group, such as translations or rotations. Our goal is to learn an equivariant representation with respect to this group action.

Formally, let  $T^k$  denote a transformation applied in the input space, parameterized by  $k$ , and let  $\hat{T}^k$  denote the corresponding transformation acting on the representation space. We seek an encoder  $f_E$  such that

$$f_E(T^k x) = \hat{T}^k f_E(x), \quad (5)$$

or equivalently,

$$T^k x = f_E^{-1}(\hat{T}^k f_E(x)), \quad (6)$$

where  $f_E^{-1}$  denotes a (possibly implicit) decoder. Although  $T^k$  and  $\hat{T}^k$  are parameterized by the same group element, they need not share the same functional form.

One approach to achieving equivariance is to explicitly map representations to a canonical pose, thereby factoring out the effect of the transformation. This perspective motivates the use of a *shift operator* Bouchacourt et al., 2021, which models the group action in the representation space. Concretely, the shift operator, which has the same dimensionality as the latent embedding, is constructed in Kronecker product form using the building block  $M$ :

$$M^k := \begin{bmatrix} 0 & 0 & \cdots & 1 \\ 1 & 0 & \cdots & 0 \\ 0 & 1 & 0 & \cdots \\ \vdots & & \ddots & \vdots \\ 0 & \cdots & 1 & 0 \end{bmatrix}^k \quad (7)$$

The matrix  $M$  corresponds to the elementary generator of the transformation group and has size equal to the order of the group. For a shift of degree  $n$ , the corresponding shift operator is obtained by applying the elementary shift  $n$  times, which is equivalent to using the matrix power  $M^n$  as the building block along the diagonal.

Under this formulation, sequential transformations compose additively in the representation space. In particular, for two transformations  $T^{k_1}$  and  $T^{k_2}$ , we have

$$T^{k_2} T^{k_1} x = f_E^{-1}(M^{k_2} M^{k_1} f_E(x)) = f_E^{-1}(M^{k_1+k_2} f_E(x)), \quad (8)$$

which reflects the underlying group structure.

Importantly, the shift operator formulation does not require explicit knowledge of the transformation parameter applied to each input. Instead, it only assumes knowledge of the cycle order of the transformation group, making it well suited to scenarios with limited or missing transformation supervision.

### A.2 EXTRAPOLATION WITH SHIFT OPERATOR

Extrapolation refers to making predictions on regions of the input domain that lie outside the range observed during training, in contrast to interpolation, which concerns predictions within the training domain. To study extrapolation under controlled conditions, we restrict the range of shift transformations observed during training in two ways.

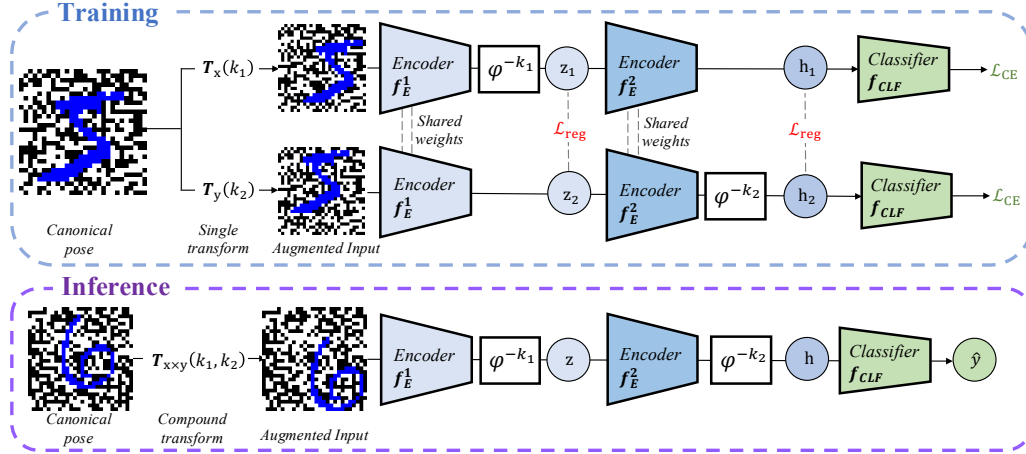


Figure 4: **Pipeline of operator-based classification under compound transformations.** Top (Training): A canonical input is transformed along individual axes to generate augmented views. Shared encoders map each view into a representation space, where inverse operators  $\varphi^{-k}$  align embeddings back to a canonical pose. Bottom (Inference): Given an input undergoing a compound transformation  $T_{x,y}(k_1, k_2)$ , the model encodes the input and applies the corresponding inverse operators to recover a canonical representation for classification.

Firstly, Section A.2.1 discusses transformations along a single degree of freedom (e.g., rotation or translation along one axis). In this case, although the full transformation group contains  $N$  discrete degrees, we train the model using only a subset of  $N_{\text{train}} < N$  transformation degrees and evaluate on the remaining unseen degrees.

Secondly, Section A.2.1 elaborates on transformations along multiple dimensions (*compound transformation*), for which we restrict the set of transformation pairs to a strict subset of the full Cartesian product:  $\mathcal{K}_{\text{train}} \subset \mathcal{K}_x \times \mathcal{K}_y$ . Evaluation is then performed on unseen compositions  $(\mathcal{K}_x \times \mathcal{K}_y) \setminus \mathcal{K}_{\text{train}}$ , which tests the model’s ability to generalize to novel combinations of transformations.

### A.2.1 Single transformation

We first study extrapolation under a single transformation dimension. During training, the model is exposed to only a restricted subset of transformation degrees, while evaluation is performed on unseen degrees outside this range. This setting directly tests whether the learned operator captures the underlying transformation structure rather than merely interpolating within the observed range.

From the perspective of group theory, many transformation families form a cyclic group whose elements are generated by repeated application of an elementary operator. Because group actions are closed under composition, transformations outside the training range can be expressed as compositions of transformations seen during training. Consequently, if the model learns the correct group action for a subset of elements, it can extrapolate to unseen transformations via recursive application of the same operator.

### A.2.2 Compound transformation

In many practical settings, inputs undergo transformations that are compositional rather than separate, such as simultaneous translations along multiple axes. We refer to such cases as *compound transformations*, where the overall transformation can be expressed as the composition of multiple elementary operators.

A direct approach would be to learn a distinct operator for every possible combination of transformations. However, this quickly becomes impractical: if there are  $M$  transformation types, each

with  $N$  discrete variants, exhaustively observing all compound transformations requires  $O(N^M)$  transformation instances. This not only leads to a combinatorial explosion in the number of operators, but also substantially increases the dimensionality of the latent representation.

Compound transformations can instead be decomposed into elementary components. Prior latent operator approaches Bouchacourt et al. (2021) employ stacked shift operators to sequentially undo each transformation, ensuring that the number of operators scales with the order of each elementary group. However, the method proposed in Bouchacourt et al. (2021) was trained on all possible compound poses, which incurs the same quadratic data requirement: observing all compositions requires  $O(N^M)$  samples.

In contrast, our approach trains the model using only single-axis transformations, as denoted in Figure 4. During training, we expose the model only to individually transformed views along each axis. For a training sample  $x$  and two transformation  $T_x, T_y$ , we generate

$$x_x = T_x^{k_1}(x), \quad x_y = T_y^{k_2}(x),$$

and obtain their canonicalized embeddings by applying the corresponding inverse operators:

$$Z_x = \varphi_x^{-k_1} f_E(x_x), \quad Z_y = \varphi_y^{-k_2} f_E(x_y).$$

Consistency is enforced between these canonical representations using the same regularization objective as in the single-transformation case:

$$\mathcal{L}_{\text{reg}} = \|Z_x - Z_y\|_2^2, \tag{9}$$

while classification is performed on the canonicalized embedding.

This encourages the encoder to learn representations that are aligned under each elementary transformation. Although this separate transformation was technically compatible with Bouchacourt et al. (2021), the feasibility of learning compound transformations via exposure to single transformations during training exclusively was not explored.

At inference time, when the input is subject to a known compound transformation, similar to (Bouchacourt et al., 2021), we sequentially apply the corresponding inverse operators to recover a canonical representation before classification. By exploiting the compositional reuse of operator blocks, our method reduces both the size of the operator space and the number of required transformation observations from  $O(N^M)$  to  $O(NM)$ , while handling compound transformations without introducing additional parameters or retraining.

### A.3 LEARNED OPERATOR

The hard-coded constructions presented in Section A.1 demonstrate the existence of a valid operator that satisfies the desired transformation behavior for this task. While these fixed operators provide a constructive proof of feasibility, they are not necessarily optimal when integrated into a larger learning pipeline. To allow the operator to adapt to the data and interact with other learned components, we parameterize the operator and optimize it jointly with the rest of the model.

In this setting, the true order of the transformation group may be unknown. We therefore fix the size of the operator building block to match the latent dimensionality, which serves as an upper bound on the transformation order. This design allows the learned operator to represent transformations of varying effective orders within a fixed-dimensional latent space.

## B IMPLEMENTATION DETAILS

We use the standard train/test split of the MNIST dataset (LeCun et al., 2010), further partitioning the training set into training and validation subsets with an 80/20 split. For background generation, we sample an independent random checkerboard for each image by uniformly assigning each cell in the  $28 \times 28$  grid to either black or white. Rotations are applied to the digit mask using nearest-neighbor resampling with zero padding to preserve discrete pixel structure. For translations, we use circular shifts implemented via array rolling, thereby pixels shifted beyond the image boundary

Table 1: **Classification accuracy (%) under translation extrapolation.** Results for horizontal (x-axis) and vertical (y-axis) shifts. “Degree given” indicates whether the true translation degree is provided at test time. Blue-shaded columns denote degrees seen during training; unshaded columns are unseen.

Operator	Degree given	k	Degree													
			-12	-10	-8	-6	-4	-2	0	2	4	6	8	10	12	14
<b>Translation on y-axis</b>																
×	-	-	18.151	18.519	21.299	45.145	78.490	83.016	83.294	83.072	79.613	51.129	23.357	13.602	15.182	16.717
Fixed	✓	-	95.885	95.985	95.996	95.952	96.018	96.185	96.063	96.074	95.751	96.018	95.807	95.707	95.629	95.707
Fixed	×	1	93.816	93.872	93.816	93.849	94.061	94.216	94.094	94.183	93.894	93.861	93.638	93.616	93.872	93.683
Fixed	×	3	93.594	93.849	93.938	93.861	94.150	94.261	94.606	93.894	93.282	93.582	93.427	93.638	93.538	93.293
Fixed	×	10	93.605	93.727	93.916	93.916	94.061	94.194	94.161	94.372	93.816	93.705	93.516	93.571	93.438	93.582
Learned	✓	-	94.628	95.329	95.429	96.185	96.274	95.840	95.985	96.040	96.263	96.118	95.373	95.106	94.951	94.773
Learned	×	1	91.347	91.736	91.758	92.626	92.782	92.025	91.914	94.061	93.838	93.082	92.137	92.148	91.425	91.425
Learned	×	3	74.964	78.167	87.543	92.726	93.749	93.193	92.626	93.594	92.871	91.970	89.245	83.172	73.540	70.626
Learned	×	10	74.830	79.324	88.233	92.715	93.182	91.758	91.380	94.150	93.449	92.237	88.311	81.771	72.506	69.614
<b>Translation on x-axis</b>																
×	-	-	33.556	44.144	61.628	78.501	87.543	89.323	89.456	89.345	88.166	80.080	59.426	38.805	29.619	28.262
Fixed	✓	-	93.582	94.595	95.262	95.863	95.907	95.918	95.718	96.018	95.974	95.974	95.596	94.862	93.827	92.270
Fixed	×	1	91.158	92.548	93.360	94.116	94.305	94.150	94.127	94.450	94.394	94.305	94.038	92.670	91.247	89.578
Fixed	×	3	91.859	92.014	92.048	92.526	93.160	92.615	93.204	93.638	93.071	92.771	92.070	92.159	91.603	91.580
Fixed	×	10	90.869	91.469	91.414	91.792	92.148	91.336	91.647	94.272	93.160	92.626	91.603	91.614	91.002	91.625
Learned	✓	-	86.498	86.865	92.159	95.462	96.029	95.707	95.618	95.762	95.685	94.684	93.004	89.634	83.628	83.684
Learned	×	1	76.543	79.391	88.377	93.004	93.627	92.492	92.181	94.150	93.616	92.370	89.434	82.894	74.063	71.716
Learned	×	3	74.964	78.167	87.543	92.726	93.749	93.193	92.626	93.594	92.871	91.970	89.245	83.172	73.540	70.626
Learned	×	10	74.830	79.324	88.233	92.715	93.182	91.758	91.380	94.150	93.449	92.237	88.311	81.771	72.506	69.614

Table 2: **Classification accuracy (%) under rotation extrapolation.** “Degree given” indicates whether the true rotation degree is provided at test time. Blue-shaded columns denote degrees seen during training; unshaded columns are unseen.

Operator	Degree given	k	Degree									
			-144	-108	-72	-36	0	36	72	108	144	180
×	-	-	25.170	30.620	74.497	78.456	77.322	79.001	75.075	31.721	26.148	25.648
Fixed	✓	-	95.707	95.751	95.785	95.963	95.918	95.707	95.607	95.696	95.618	95.840
Fixed	×	1	86.042	85.841	86.753	86.965	86.842	86.976	86.720	85.975	85.875	86.564
Fixed	×	3	86.920	87.521	88.644	89.523	89.890	86.831	84.763	84.051	84.740	85.864
Fixed	×	10	87.298	87.443	87.721	88.099	88.511	89.834	88.377	87.821	87.843	87.810
Learned	✓	-	95.774	96.052	96.185	96.129	96.118	96.018	96.285	95.762	95.284	95.718
Learned	×	1	86.242	85.586	85.853	85.452	85.363	89.256	88.655	87.443	86.753	86.742
Learned	×	3	87.321	87.554	88.032	88.121	88.544	89.078	87.588	86.709	85.797	86.553
Learned	×	10	86.609	85.719	86.609	86.119	86.865	91.180	90.023	88.967	87.866	87.588

reappear on the opposite side rather than being clipped. The transformed digit mask is then overlaid onto the random background.

Upon loading, images are normalized to the range  $[0,1]$  and flattened from  $3 \times 28 \times 28$  into a 2,352-dimensional feature vector. A linear encoder then maps this vector to a latent representation of dimension 70, which is also the dimensionality of the transformation operators. In the presence of transformations, the latent embedding is manipulated with the linear operator in the representation space. For compound transformations, the second encoder is a linear mapping of size  $70 \times 70$  to adapt the canonical representation to the second transformation before canonicalizing.

All models are trained using the Adam optimizer with a learning rate of 0.001 and a batch size of 512 for 20 epochs and temperature  $\lambda = 1$  in Eq.2. All experiments are conducted on a single NVIDIA RTX 5090 desktop GPU.

In the evaluation reported in Figure 2 the appropriate operator was chosen by our k-NN methods. To that end, we shuffle the validation set using a fixed random seed (42), select 2,000 samples as the reference set, and perform nearest-neighbor classification with  $k = 1$ .

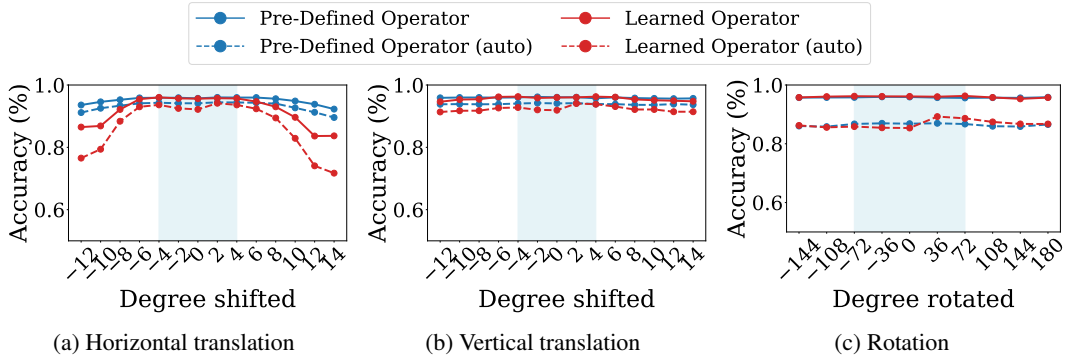


Figure 5: **Extrapolation behavior of operator-based models on MNIST.** Solid lines use ground-truth transformation degrees; dashed lines “(auto)” use k-NN pose inference. Shaded regions denote training degrees.

## C ADDITIONAL RESULTS

### C.1 EXTRAPOLATION RESULTS

We report the absolute numerical accuracy for the extrapolation test visualized in Figure 2 in Table 1 and Table 2. The shaded columns indicate transformation degrees observed during training, while unshaded columns correspond to unseen (out-of-distribution) transformations.

We observe that the baseline model without operators experiences a severe accuracy degradation as the amount of distortion deviates substantially from the learned set. Although its performance is moderate within the observed region, accuracy drops sharply for larger unseen shifts and rotations, in some cases approaching near-random levels. This behavior indicates that the baseline fails to generalize beyond the transformation degrees encountered during training and must implicitly absorb transformation variability into its representation. For example, under vertical translation (along y-axis), baseline accuracy drops from 78.5–83.3% within the observed region to 13.6% at a shift of +10 and 15.2% at +12. Under rotation, the degradation is also pronounced: accuracy falls from 78–79% in-domain to 25–31% at extreme angles ( $\pm 144^\circ$ ,  $180^\circ$ ). This sharp decline indicates poor extrapolation beyond the transformation degrees seen during training.

In contrast, operator-based models maintain stable performance across the full transformation range. When the true transformation is provided at test time (“Degree given”  $\checkmark$ ), both fixed and learned operators achieve near-constant accuracy of 95–96% across all translation and rotation degrees, including unseen ones. Even when the transformation must be inferred (“Degree given”  $\times$ ), performance remains high. For example, under rotation with automatic inference ( $k=1$ ), accuracy remains around 85–87% across all angles—dramatically outperforming the baseline at extreme rotations. Similar stability is observed for translations, where operator models consistently remain above 90% even far outside the training range.

Figure 5 illustrates the accuracy behavior of operator-based models as a function of transformation magnitude. The results show that strong out-of-distribution performance is consistent for both pre-defined (blue) and learned (red) operators. The flat accuracy curves outside the shaded training region indicate that the operator formulation successfully generalizes beyond the observed transformation range. The similarity between pre-defined and learned operators suggests that the robustness stems from the operator-based factorization itself rather than a particular parameterization.

### C.2 ABLATION: HYPERPARAMETERS FOR K-NN SEARCH

We conduct an ablation to study the impact of reference set size  $N$  and neighborhood size  $k$  on k-NN search accuracy. For each  $N \in \{100, 200, 500, 1000, 2000, 5000\}$ , we randomly sample a reference set and extract canonicalized embeddings using the optimized model. Test samples at each discrete transformation degree are classified via kNN search over the reference embeddings, with  $k \leq N$ . The results reported in Tables 3, 4, and 5 are averaged across multiple random seeds  $\{0, 10, 20, 30, 42\}$  and all possible transformation degrees.

Table 3: **k-NN performance on rotated MNIST.**  $\text{Acc}_{\text{pose}} (\uparrow)$  and  $\text{Acc}_{\text{cls}} (\uparrow)$  denote pose prediction and downstream classification accuracy, respectively. **GT** reports the reference performance with ground-truth poses.

$k$	$N$											
	100		200		500		1000		2000		5000	
	$\text{Acc}_{\text{pose}}$	$\text{Acc}_{\text{cls}}$										
<b>GT</b>	100.000	95.759	100.000	95.759	100.000	95.759	100.000	95.759	100.000	95.759	100.000	95.759
1	<b>54.196</b>	<b>76.136</b>	60.339	<b>80.185</b>	65.292	83.375	68.912	85.473	71.543	87.029	74.159	88.726
3	51.829	73.990	59.669	79.097	66.285	83.136	70.421	85.512	73.273	87.171	75.949	88.940
10	53.287	75.149	<b>61.767</b>	80.054	<b>68.687</b>	<b>84.356</b>	<b>72.950</b>	<b>86.649</b>	<b>75.746</b>	<b>88.117</b>	<b>78.735</b>	<b>89.771</b>
30	49.344	72.227	58.294	77.425	66.211	82.657	71.258	85.480	74.676	87.288	78.143	89.172
100	40.792	66.761	50.160	72.366	59.804	78.436	65.642	82.134	70.056	84.612	74.985	87.326
300	–	–	–	–	51.437	73.311	58.320	77.275	63.375	80.187	69.657	84.169

Table 4: **k-NN performance on x-translated MNIST.**  $\text{Acc}_{\text{pose}} (\uparrow)$  and  $\text{Acc}_{\text{cls}} (\uparrow)$  denote pose prediction and downstream classification accuracy, respectively. **GT** reports the reference performance when ground-truth poses were given. The highest score for each  $N$  is shown in **bold**.

$k$	$N$											
	100		200		500		1000		2000		5000	
	$\text{Acc}_{\text{pose}}$	$\text{Acc}_{\text{cls}}$										
<b>GT</b>	100.000	95.097	100.000	95.097	100.000	95.097	100.000	95.097	100.000	95.097	100.000	95.097
1	<b>65.661</b>	<b>86.931</b>	<b>71.705</b>	<b>89.458</b>	76.762	<b>91.406</b>	79.852	<b>92.351</b>	82.816	<b>93.049</b>	85.395	<b>93.652</b>
3	61.803	84.460	69.530	88.018	76.752	90.774	80.566	91.964	83.767	92.776	86.307	93.501
10	59.041	82.852	68.694	87.245	<b>77.251</b>	90.438	<b>81.514</b>	91.884	<b>84.657</b>	92.752	<b>87.464</b>	93.488
30	49.978	77.833	62.427	83.570	73.384	88.400	79.318	90.649	83.263	91.986	86.501	92.973
100	35.470	69.169	44.566	75.132	62.005	83.197	71.753	87.313	77.801	89.653	83.078	91.734
300	–	–	–	–	44.389	74.927	58.429	81.770	68.581	85.535	76.887	89.191

Table 5: **k-NN performance on y-translated MNIST.**  $\text{Acc}_{\text{pose}} (\uparrow)$  and  $\text{Acc}_{\text{cls}} (\uparrow)$  denote pose prediction and downstream classification accuracy, respectively. **GT** reports the reference performance when ground-truth poses were given. The highest score for each  $N$  is shown in **bold**.

$k$	$N$											
	100		200		500		1000		2000		5000	
	$\text{Acc}_{\text{pose}}$	$\text{Acc}_{\text{cls}}$										
<b>GT</b>	100.000	95.913	100.000	95.913	100.000	95.913	100.000	95.913	100.000	95.913	100.000	95.913
1	<b>66.732</b>	<b>87.442</b>	<b>72.056</b>	<b>90.092</b>	77.052	<b>92.161</b>	79.872	<b>93.020</b>	82.513	<b>93.792</b>	85.342	<b>94.532</b>
3	63.211	84.416	71.428	88.416	77.668	91.441	80.967	92.725	83.756	93.651	86.227	94.502
10	62.334	84.603	71.036	88.648	<b>78.322</b>	91.380	<b>82.019</b>	92.753	<b>84.673</b>	93.655	<b>87.319</b>	94.521
30	57.436	83.192	66.505	86.956	76.085	90.423	80.460	91.934	83.504	93.067	86.603	94.138
100	47.862	78.718	55.208	82.766	67.933	87.820	75.309	90.169	80.057	91.618	83.930	93.080
300	–	–	–	–	56.196	83.258	64.537	86.892	73.189	89.365	79.839	91.525

**Effect of reference set size.** Across all transformations, both pose prediction accuracy ( $\text{Acc}_{\text{pose}}$ ) and downstream MNIST classification accuracy ( $\text{Acc}_{\text{cls}}$ ) improve consistently as the reference set size  $N$  increases, since larger reference sets provide denser coverage of the canonical embedding space, and hence more reliable nearest-neighbor retrieval. However, performance gains begin to saturate between  $N = 2000$  and  $N = 5000$ .

**Effect of neighborhood size  $k$ .** There appears to be a clear non-monotonic effect on performance in terms of  $k$ . The performance exhibits a clear non-monotonic dependence on  $k$ . Indeed, large neighborhoods ( $k \geq 100$ ) dilute pose-specific information. Interestingly, even very small neighborhoods (e.g.,  $k = 1$ ) can often infer the correct pose, indicating that nearest matches in the embedding space are reliably informative. Across all transformations, a moderate value of  $k$ , most notably  $k = 10$ , consistently achieves the highest  $\text{Acc}_{\text{pose}}$  and  $\text{Acc}_{\text{cls}}$ , potentially thanks to its robustness against noisy outliers and local pose structure.

**Comparison across transformations.** Despite the larger group order, translation-based tasks are generally easier than rotation, achieving higher pose and classification accuracy under identical

$(N, k)$  configurations. Nevertheless, we chose  $N = 2000$  as the accuracy for finding the correct pose is typically around 70–80% and leads to negligible degradation in the downstream score.

**Using ground-truth transformations as labels.** We performed an ablation where the ground-truth transformation was provided at test time, and used as transformation label instead of the automatic k-NN pose inference label. As illustrated in Figure 5, automatic inference (dashed lines) yields slightly lower accuracy than the supervised inference with the ground-truth operator (solid lines), yet the performance gap remains modest across most transformation degrees. This result suggests that the model learns a well-structured latent space in which samples are correctly mapped to their canonical version through application of the latent operator, leading to robust pose estimation, disentanglement, and extrapolation.

**Future work.** Overall, predicted poses were not entirely correct, but the degradation remained small for several choices of hyperparameters. Notwithstanding this empirical success, our current pose prediction procedure does not scale well, as it relies on an exhaustive search over transformation candidates and distance comparisons against a selected reference set. This results in complexity that grows with both the number of transformation degrees and the size of the reference database. Future work could alleviate this limitation by developing more structured inference mechanisms—such as learning transformation-aware embeddings/classifiers or exploiting spectral decompositions—so that the pose can be inferred in linear time with respect to the embedding dimension rather than the transformation space.